The Astronomical Journal, 148:24 (10pp), 2014 July doi:10.1088/0004-6256/148/1/24

EXTINCTION MAPS TOWARD THE MILKY WAY BULGE: TWO-DIMENSIONAL AND THREE-DIMENSIONAL TESTS WITH APOGEE

M. Schultheis[1], G. Zasowski[2,20], C. Allende Prieto[3,4], F. Anders[5,6], R. L. Beaton[7], T. C. Beers[8,9], D. Bizyaev[10,11], C. Chiappini[5,12], P. M. Frinchaboy[13], A. E. García Pérez[7], J. Ge[14], F. Hearty[15], J. Holtzman[11], S. R. Majewski[7], D. Muna[16], D. Nidever[17], M. Shetrone[18], and D. P. Schneider[15,19]

[1] Université de Nice Sophia-Antipolis, CNRS, Observatoire de Côte d'Azur, Laboratoire Lagrange, 06304 Nice Cedex 4, France; mathias.schultheis@oca.eu
[2] Department of Physics & Astronomy, Johns Hopkins University, Baltimore, MD 21218, USA; gail.zasowski@gmail.com
[3] Instituto de Astrofísica de Canarias, Calle Vía Láctea s/n, E-38205 La Laguna, Tenerife, Spain
[4] Departamento de Astrofísica, Universidad de La Laguna, E-38206 La Laguna, Tenerife, Spain
[5] Leibniz-Institut für Astrophysik Potsdam (AIP), D-14482 Potsdam, Germany
[6] Technische Universität Dresden, Institut für Kern-und Teilchen-physik, D-01069 Dresden, Germany
[7] Department of Astronomy, University of Virginia, Charlottesville, VA 22904, USA
[8] National Optical Astronomy Observatory, Tucson, AZ 85719, USA
[9] Joint Institute for Nuclear Astrophysics (JINA), Michigan State University, East Lansing, MI 48824, USA
[10] Apache Point Observatory, Sunspot, NM 88349, USA
[11] New Mexico State University, Las Cruces, NM 88003, USA
[12] Laboratório Interinstitucional de e-Astronomia, -LIneA, Rio de Janeiro, RJ-20921-400, Brazil
[13] Department of Physics & Astronomy, Texas Christian University, TCU Box 298840, Fort Worth, TX 76129, USA
[14] Astronomy Department, University of Florida, Gainesville, FL 32611, USA
[15] Department of Astronomy and Astrophysics, The Pennsylvania State University, University Park, PA 16802, USA
[16] Department of Astronomy, The Ohio State University, Columbus, OH 43210, USA
[17] Department of Astronomy, University of Michigan, Ann Arbor, MI 48109, USA
[18] McDonald Observatory, The University of Texas at Austin, Austin, TX 78712, USA
[19] Institute for Gravitation and the Cosmos, The Pennsylvania State University, University Park, PA 16802, USA
Received 2014 January 27; accepted 2014 May 7; published 2014 June 13

ABSTRACT

Galactic interstellar extinction maps are powerful and necessary tools for Milky Way structure and stellar population analyses, particularly toward the heavily reddened bulge and in the midplane. However, due to the difficulty of obtaining reliable extinction measures and distances for a large number of stars that are independent of these maps, tests of their accuracy and systematics have been limited. Our goal is to assess a variety of photometric stellar extinction estimates, including both two-dimensional and three-dimensional extinction maps, using independent extinction measures based on a large spectroscopic sample of stars toward the Milky Way bulge. We employ stellar atmospheric parameters derived from high-resolution *H*-band Apache Point Observatory Galactic Evolution Experiment (APOGEE) spectra, combined with theoretical stellar isochrones, to calculate line-of-sight extinction and distances for a sample of more than 2400 giants toward the Milky Way bulge. We compare these extinction values to those predicted by individual near-IR and near+mid-IR stellar colors, two-dimensional bulge extinction maps, and three-dimensional extinction maps. The long baseline, near+mid-IR stellar colors are, on average, the most accurate predictors of the APOGEE extinction estimates, and the two-dimensional and three-dimensional extinction maps derived from different stellar populations along different sightlines show varying degrees of reliability. We present the results of all of the comparisons and discuss reasons for the observed discrepancies. We also demonstrate how the particular stellar atmospheric models adopted can have a strong impact on this type of analysis, and discuss related caveats.

Key words: dust, extinction – Galaxy: bulge – Galaxy: stellar content – Galaxy: structure

Online-only material: color figures, machine-readable table and VO tables

1. INTRODUCTION

Interstellar extinction remains one of the primary obstacles to studying the structure and stellar populations of the Galactic bulge. Some of the earliest bulge extinction maps were made using optical photometry, primarily of red clump (RC) stars, from microlensing surveys such as OGLE and MACHO (e.g., Stanek 1996; Sumi 2004; more recently Kunder et al. 2008; Nataf et al. 2013). With the arrival of large area, near-infrared (IR) photometric surveys such as DENIS and Two Micron All Sky Survey (2MASS), additional extinction maps became available. For example, Schultheis et al. (1999) and Dutra et al. (2003) used red giant branch (RGB) stars, together with stellar evolutionary models, to trace extinction up to $A(V) \sim 25$ mag with a spatial resolution of 4′. Gosling et al. (2006) used the near-IR colors of bulge stars to trace small scale interstellar dust variations (∼5″) in the Galactic Center. Gonzalez et al. (2012) also used RC stars to trace the interstellar dust extinction based upon data from the VISTA Variables in the Via Lactea (VVV) survey, which reaches sufficiently faint magnitudes to use the RC population even in the most highly extinguished regions, such as the Galactic Center. However, these extinction maps are two-dimensional, and when applying them, one implicitly assumes that all stars are located at a distance beyond the typical distance probed by the map. At the level of individual stars, Majewski et al. (2011) introduced the "Rayleigh–Jeans Color Excess" (RJCE) method, and demonstrated that near- to mid-IR colors (e.g., $H-4.5\,\mu$m) could be used to measure the effects of

[20] NSF Astronomy & Astrophysics Postdoctoral Fellow.

the interstellar dust on a star-by-star basis, largely independent of stellar type.

Only a few three-dimensional extinction maps toward the Galactic bulge area have been constructed thus far. Drimmel et al. (2003) built a theoretical three-dimensional Galactic dust distribution model, based on the interstellar dust and stellar distribution inferred from the *COBE* near- and far-IR emission. Marshall et al. (2006) provided a three-dimensional dust extinction map by comparing 2MASS data with the Besançon stellar population synthesis model (Robin et al. 2003). An improved version of the Marshall et al. map, using VVV and GLIMPSE-II data and an updated version of the Besançon model (Robin et al. 2012), has been published by Chen et al. (2013); this was later expanded by Schultheis et al. (2014) for the full VVV bulge area.

In this paper, we use stellar properties derived from new, high-resolution, near-IR spectra to probe the inner Milky Way's interstellar extinction in three dimensions, and compare the results with existing two-dimensional and three-dimensional extinction maps. This allows, for the first time, a detailed comparison of the derived extinction and distances with the available three-dimensional maps in the literature. In Section 2, we outline the sample of stars used in this study, and in Section 3, we describe the derivation of their extinctions and distances. In Sections 4 and 5, we compare these extinctions to existing two-dimensional and three-dimensional extinction maps, respectively, and present explanations for the discrepancies, including a discussion of systematic differences as a function of stellar parameters. Finally, in Section 6, we discuss the impact of the choice of stellar models and extinction law on our results.

2. THE SAMPLE

2.1. APOGEE

One of four experiments in the Sloan Digital Sky Survey III (SDSS-III; Eisenstein et al. 2011), the Apache Point Observatory Galactic Evolution Experiment (APOGEE; Majewski et al. 2010) is a large-scale, near-IR, high-resolution ($R \sim 22{,}500$) spectroscopic survey of Milky Way stellar populations. The survey uses a dedicated, 300 fiber, cryogenic spectrograph coupled to the wide-field, Sloan 2.5 m telescope (Gunn et al. 2006) at Apache Point Observatory (APO). APOGEE observes in the H band (1.5–1.7 μm), where extinction by dust is significantly lower than at optical wavelengths (e.g., $A(H)/A(V) \sim 0.16$). APOGEE observes, at high signal-to-noise ratio (S/N $\sim$ 100 per Nyquist-sampled pixel), about 100,000 red giant stars selected from the 2MASS survey, down to a typical flux limit of $H \sim$ 12–14 (Zasowski et al. 2013). Approximately 85% of our bulge stars have a magnitude brighter than $H < 11$, and all have $H < 12.2$.

Stars are observed using standard SDSS plug-plates, which normally have a field of view (FOV) radius of 1.°5, but the high airmass of the bulge observed from APO (latitude $\sim 32^\circ$) produces strong differential refraction effects on stars near the plug-plate edges. Therefore, APOGEE's bulge fields have stars no more than 0.°9 from the field center (some fields observed early in the survey are even smaller, with $R < 0.°5$) to mitigate this effect.

With its high resolution and high S/N, APOGEE will determine both accurate radial velocities (to better than 0.5 km s^{-1} external accuracy) and precise abundance measurements for most of the vast stellar sample, including the most abundant metals in the universe (C, N, O), along with other α, odd-Z, and iron-peak elements. The latest SDSS-III Data Release (DR10; Ahn et al. 2014) provides spectra of about 55,000 stars to the scientific community, as well as the derived stellar properties, including radial velocities, effective temperatures, surface gravities, and metallicities. Additional information, such as photometry and target selection criteria, is also provided and described in Zasowski et al. (2013).

2.2. Stellar Parameters

Stellar parameters are determined by the APOGEE Stellar Parameters and Chemical Abundances Pipeline (ASPCAP; Garcia Perez et al. 2014). These values are based on a χ^2 minimization between observed and synthetic model spectra performed with the FERRE code (Allende Prieto et al. 2006 and subsequent updates). Model spectra are interpolated on a regular grid computed with the ASSϵT code (Koesterke et al. 2008; Koesterke 2009), a custom line list specially compiled for the survey (M. Shetrone et al., in preparation), and Castelli & Kurucz (2004) model atmospheres. New ATLAS9 model atmospheres computed by Mészáros et al. (2012) with varying C and α content, relative to the solar composition from Asplund et al. (2005), will be used in future data releases.

The accuracy of the DR10 ASPCAP $T_{\rm eff}$, $\log g$, and [M/H] values was evaluated by Mészáros et al. (2013). Using a sample of well-studied field and cluster stars, including a large number of stars with asteroseismic stellar parameters from NASA's *Kepler* mission (Borucki et al. 2010), they compared ASPCAP results to the literature values. They conclude that the ASPCAP temperatures agree with other spectroscopic temperatures from the literature, with a mean offset of only 8 K and a 1σ scatter of 161 K. For literature photometric temperatures derived with the Infrared Flux Method (González Hernández & Bonifacio 2009), larger systematic differences were found, and a correction function was provided to convert the ASPCAP temperatures to photometrically calibrated temperatures. In the present work, we adopt the raw ASPCAP spectroscopic temperatures because these estimates, based on continuum-normalized spectra, are independent of the interstellar extinction.

ASPCAP surface gravities are, in general about 0.2–0.3 dex larger than both isochrone and seismic values in the range $-0.5 <$ [M/H] $< +0.1$, with increasing offsets at lower metallicities. An empirical correction has been calculated for use in our analysis. Metallicities agree with literature values for $-0.5 <$ [M/H] $< +0.1$ (within 0.1 dex), but at both the metal-poor and metal-rich end, systematic offsets of up to 0.2–0.3 dex are apparent. Again, a correction factor has been derived, which is applied here.

In summary, we adopt for our analysis the spectroscopic temperatures (not corrected) from ASPCAP and apply the correction terms given in Mészáros et al. (2013) for the ASPCAP surface gravities and metallicities.

2.3. Sample Used in This Work

The initial selection for our sample comprises all APOGEE targets from the first two years of the survey that are located toward the Galactic bulge: $-10^\circ < l < 10^\circ$ and $-10^\circ < b < 5^\circ$, coinciding with the footprint of the VVV survey extinction map (Gonzalez et al. 2012). These include data that are part of DR10 (comprising 60% of the sample), along with data not included in that release. For all stars, we use parameters from the v400 version of APOGEE's combined reduction + analysis pipeline.

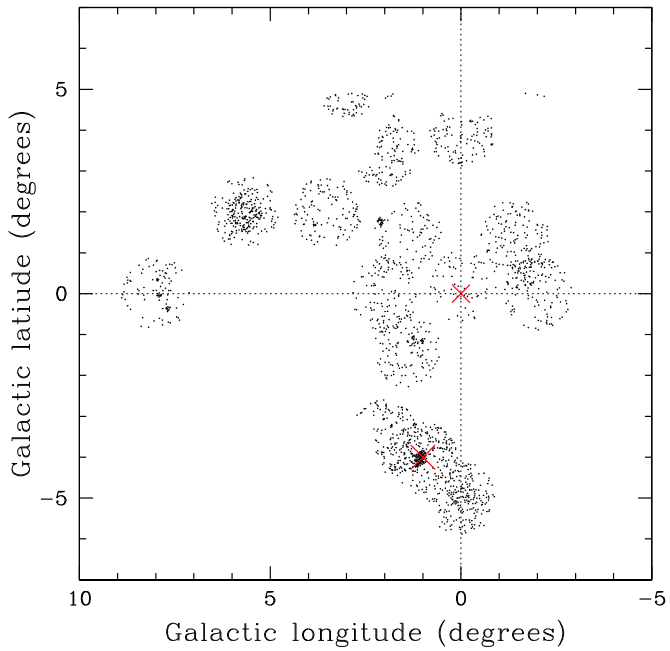

Figure 1. Galactic longitude and latitude of our final APOGEE sample toward the Galactic bulge. The positions of the Galactic Center and Baade's Window are marked with crosses.

(A color version of this figure is available in the online journal.)

We then filtered the stars to remove those with parameters close to the edges of the model grid, as described by Mészáros et al. (2013). We selected stars with S/N > 50, $\chi^2_{\rm ASPCAP} < 30$, and $\log g < 3.5$. to ensure a sample of stars with reliable ASPCAP fits and stellar parameters. No additional selection criteria in $T_{\rm eff}$ or [M/H] have been applied, though we did reject stars where these values were not well-matched by the stellar models described below (Section 3). Figure 1 shows the distribution in Galactic longitude (l) and Galactic latitude (b) of our final sample of 2433 stars.

3. DERIVATION OF EXTINCTION AND DISTANCES

We used the Padova isochrones set[21] from Marigo et al. (2008) along with the Girardi et al. (2010) Case A correction for low-mass, low-metallicity AGB tracks that were matched with the ASPCAP parameters $T_{\rm eff}$, $\log g$, and [M/H], for our sample of APOGEE targets. Our isochrone grid has metallicity steps of 0.2 dex between $-2.5 <$ [Fe/H] $< +0.5$ and age steps of $\Delta(\log \text{age}) = 0.05$ Gyr. The intrinsic Padova model grid is slightly irregular in $T_{\rm eff}$ and $\log g$ depending on the $T_{\rm eff}$ range, but the steps in mass are sufficiently small to ensure a typical resolution better than 100 K in $T_{\rm eff}$ and 0.1 dex in $\log g$. However, we note that the isochrone grid samples very poorly the parameter space within $3500 < T_{\rm eff} < 4000$ K and $\log g > 2.0$. ASPCAP estimates [M/H], not [Fe/H], using multiple elements. As pointed out by Mészáros et al. (2013), [M/H] is, in general close to [Fe/H], particularly after the Mészáros et al. (2013) calibration is applied—within 0.1 dex or so. We therefore assume that the [Fe/H] values of the isochrones are equivalent to [M/H]. For alpha-enhanced stars this relation might be not valid, and could therefore introduce additional errors in the distance and extinction determination.

For each star, we selected the isochrone closest in metallicity and then identified the closest point in the corresponding $T_{\rm eff}$ and $\log g$ plane of the isochrone. No interpolation has been done, but stars that are too far from a point in the isochrone-grid ($|\Delta T_{\rm eff}| > 500$ K or $|\Delta \log g| > 0.5$ dex) are discarded. Figure 2 shows the differences in $T_{\rm eff}$ and $\log g$ between the spectroscopic values and those of the best-matched Padova isochrone point for each star (in the sense of ASPCAP–"isochrone"). While the differences in $\log g$ are rather small (<0.025 dex), the effective temperatures can differ by several hundred K, mainly due to the irregular grid spacing in the $T_{\rm eff}$ versus $\log g$ plane of the Padova isochrones. No dependency on metallicity was found. The asymmetric tail seen in Figure 2 is composed of stars that fall in the parameter space $3500 < T_{\rm eff} < 4000$ K and $\log g > 2.0$, not covered by the isochrone grid. These stars comprise ~3% of the sample. As a secondary effect, α-enhanced bulge stars might not be as well represented by the assumption of [M/H] = [Fe/H] and solar-scaled isochrones.

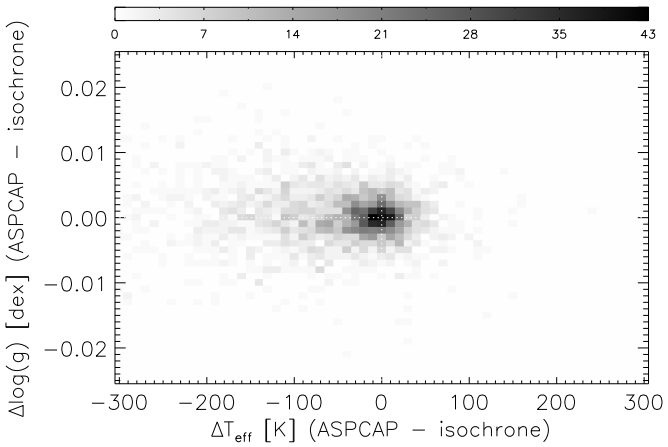

Figure 2. Difference in $T_{\rm eff}$ and $\log g$ (ASPCAP–"isochrone") of our sample. The peak in both distributions is at zero, although due to the irregular grid in $T_{\rm eff}$ and $\log g$ of the Padova isochrones, the tail of the $\Delta T_{\rm eff}$ distribution is asymmetric toward more negative values.

These $\log g$ and $T_{\rm eff}$ offsets are incorporated into the uncertainties in the final extinction and distance estimates (see below).

Each star in the APOGEE sample has 2MASS magnitudes J, H, and K_s. In the corresponding isochrone grid, we find the absolute magnitudes M_J, M_H, and M_{Ks}. The color excess $E(J-K_s)$ can then simply be calculated by $E(J-K_s) = J - K_s - (M_J - M_{Ks})$, where J and K_s are the star's observed 2MASS magnitudes and $(M_J - M_{Ks})$ the intrinsic, unreddened color from the isochrones. To convert $E(J-K_s)$ to $A(K_s)$, one has to assume a certain extinction law. We use here the relationships of Nishiyama et al. (2009), with $A(K_s) = 0.528 \times E(J-K_s)$, which was derived for sightlines near the Galactic Center. The extinction derived using this method is hereafter referred to as $A(K_s)_{\rm ASPCAP}$. Note that $A(K_s)_{\rm ASPCAP}$ is not a product of ASPCAP. The extinction law toward the Galactic bulge remains somewhat uncertain, although it has been shown to vary along different lines of sight (e.g., Gao et al. 2009; Fritz et al. 2011; Chen et al. 2013; Nataf et al. 2013). In Section 6 we examine the potential impact of these variations on our findings.

The distance between each star and the isochrone grid in the $\Delta T_{\rm eff}$ and $\Delta \log g$ dimensions (see Figure 2), together with the individual errors $\sigma_{T_{\rm eff}}$ and $\sigma_{\log g}$ from the ASPCAP pipeline (those derived empirically by Mészáros et al. 2013), give the total error in $T_{\rm eff}$ and $\log g$ for each star:

$$\text{err}_{T_{\rm eff}} = \sqrt{\Delta T_{\rm eff}^2 + \sigma_{T_{\rm eff}}^2} \quad \text{and} \quad \text{err}_{\log g} = \sqrt{(\Delta \log g)^2 + \sigma_{\log g}^2}.$$

[21] http://stev.oapd.inaf.it/cgi-bin/cmd

Table 1
Derived Extinction and Distances from Our APOGEE Sources

Object	R.A. (deg)	Decl. (deg)	$A(K_s)$ (mag)	$\sigma(A(K_s))$ (mag)	Dist. (kpc)	σ(dist.) (%)	$A(K_s)_{\rm RJCE}$ (mag)	$A(K_s)_{\rm N12}$ (mag)	$A(K_s)_{\rm G12}$ (mag)	$A(K_s)_{\rm EHK}$ (mag)
2M17515147-2215539	267.9644470	−22.2649879	0.218	0.034	7.449	59.189	0.213	0.229	0.230	0.328
2M17515740-2229440	267.9891663	−22.4955711	0.171	0.024	2.316	31.137	0.203	0.312	0.261	0.158
2M17515917-2221365	267.9965515	−22.3601379	0.238	0.037	5.140	34.498	0.254	0.263	0.244	0.344
2M17520342-2326376	268.0142822	−23.4438000	0.290	0.029	4.626	39.296	0.369	0.345	0.331	0.404
2M17520525-2248283	268.0218811	−22.8078842	0.281	0.038	6.936	46.518	0.297	0.288	0.250	0.487

(This table is available in its entirety in machine-readable and Virtual Observatory (VO) forms in the online journal. A portion is shown here for guidance regarding its form and content.)

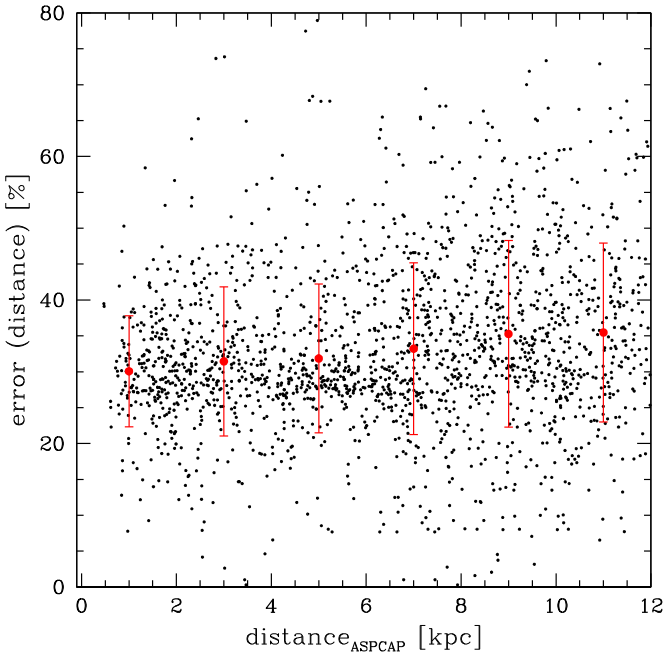

Figure 3. Fractional distance error as a function of distance. The error in the distance includes both the error in the isochrone-matching method and the typical errors in the stellar parameters derived by ASPCAP. The red points show the median values and the error bars the standard deviation in the six distance bins.

(A color version of this figure is available in the online journal.)

For each star, we added these uncertainties to the ASPCAP values (i.e., $T_{\rm eff} \pm {\rm err}_{T_{\rm eff}}$ and $\log g \pm {\rm err}_{\log g}$) and redid the isochrone matching, thus estimating the typical uncertainty in $A(K_s)_{\rm ASPCAP}$ for this method. However, these errors do not include systematic contributions from the choice of the stellar atmosphere models, isochrones, etc. We discuss this issue in Section 6.3.

Our distances were calculated using:

$$d = 10^{(0.2\times(K_s - M_{K_s})+5-A(K_s)_{\rm ASPCAP})}, \quad (1)$$

with K_s the 2MASS apparent magnitude, M_{Ks} the absolute K_s magnitude from the Padova isochrone, and the extinction $A(K_s)_{\rm ASPCAP}$ as described above. The errors in the distance are obtained in the same way as for $A(K_s)_{\rm ASPCAP}$, including the errors in $T_{\rm eff}$ and $\log g$.

The resulting median errors in our derived distances from the isochrone-matching method, including the ASPCAP errors in $T_{\rm eff}$ and $\log g$, are on the order of ∼30%–40% (see Figure 3). We compared our distances with those of Anders et al. (2014), who use a more sophisticated Bayesian approach based on Allende Prieto et al. (2008) to compute SDSS distances both for APOGEE giants and SEGUE dwarfs. In general, there is good agreement between the two distance scales. For small heliocentric distances ($d < 2$ kpc) we find smaller values than Anders et al., by about 20%, whereas for larger distances ($d > 6$ kpc) we tend to find slightly larger values. The rms scatter between our work and Anders et al. is about 30%, similar to the typical intrinsic error of our distances (Figure 3). In Table 1, we present the derived extinctions (and associated distances) for our sample, along with the extinction values based on the literature two-dimensional maps as described in the next section.

4. COMPARISON TO INDIVIDUAL STELLAR EXTINCTIONS AND TWO-DIMENSIONAL EXTINCTION MAPS

4.1. Stellar Extinction Estimates and Two-dimensional Maps Used

We compare our isochrone-based extinctions, $A(K_s)_{\rm ASPCAP}$, to the following data:

1. The individual stellar RJCE extinction estimates, $A(K_s)_{\rm RJCE}$, following the method of Majewski et al. (2011). We explored using both the *Spitzer*-IRAC 4.5 μm and the *WISE* *W2* (4.6 μm) filters (together with 2MASS *H*), but the larger pixel size of *WISE* is particularly disadvantageous in the crowded bulge, so we opt to use IRAC data exclusively for $A(K_s)_{\rm RJCE}$.
2. The individual stellar extinction estimates derived from the $E(H - K_s)$ color excess, EHK, following Lada et al. (1994), and assuming that all stars share a common intrinsic $(H - K_s)_0 = 0.13$ color. This assumption is only the first step of the fuller NICE extinction-mapping method (e.g., Lada et al. 1994; Lombardi & Alves 2001; Gosling et al. 2009), but statistically cleaned NICE maps of large bulge regions have not yet been constructed.
3. The extinction map based on RC stars by Gonzalez et al. (2012, hereafter G12). Using the BEAM calculator Web page,[22] we retrieved for each star the extinction in the map's 2′ pixel closest to the star's position, $A(K_s)_{\rm G12}$.
4. The "all stars, median" extinction map using the RJCE method by Nidever et al. (2012, hereafter N12). With the query scripts provided in that paper, we retrieved, for each star, the extinction in the 2′ pixel closest to the star's position, $A(K_s)_{\rm N12}$.

All reddening or extinction values were transformed, if necessary, to $A(K_s)$ with the extinction law of Nishiyama et al. (2009).

[22] http://mill.astro.puc.cl/BEAM/calculator.php

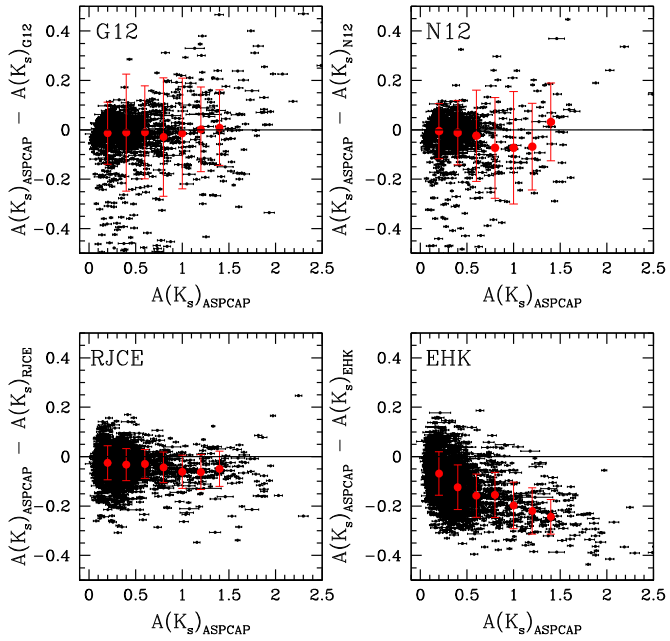

Figure 4. Comparison of our derived extinction, $A(K_s)_{\rm ASPCAP}$, to those of G12 (upper left), N12 (upper right), RJCE (lower left), and EHK (lower right), as a function of ASPCAP extinction. The error bars are the results from the isochrone matching (see text). The red points show the median values and dispersions in $A(K_s)_{\rm ASPCAP}$ bins spaced 0.2 mag apart.

(A color version of this figure is available in the online journal.)

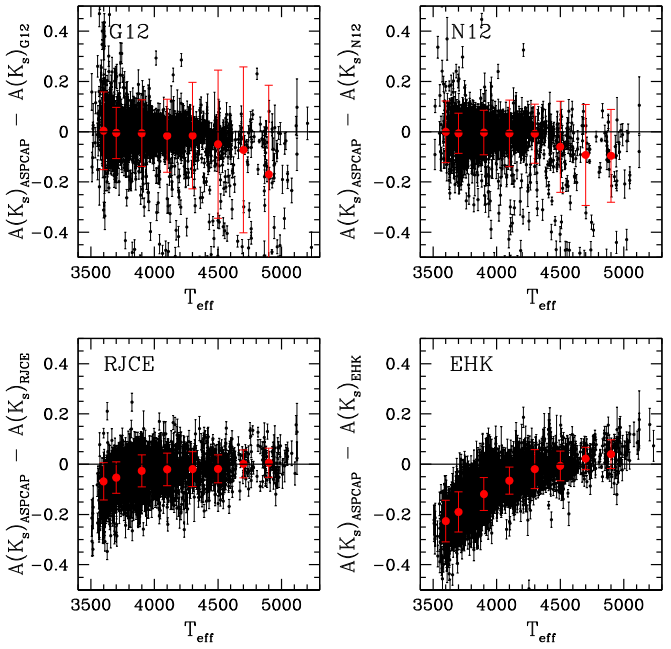

Figure 5. Comparison of our derived extinction, $A(K_s)_{\rm ASPCAP}$, to those of G12 (upper left), N12 (upper right), RJCE (lower left), and EHK (lower right), as a function of $T_{\rm eff}$. The error bars are the results from the isochrone matching (see text). The red points show the median value and dispersion.

(A color version of this figure is available in the online journal.)

4.2. Results and Discussion

Figure 4 shows the comparison of our derived extinction, $A(K_s)_{\rm ASPCAP}$, with: G12 in the upper left panel, N12 in the upper right panel, RJCE in the lower left panel, and EHK in the lower right panel. We include for each star the typical error resulting from the isochrone matching. Each panel does not include the same number of stars, due to the fact that some stars lack reliable extinction measurements from all four methods because of their inhomogeneous photometry. These stars "missing" one or more estimates have no preferred $A(K_s)_{\rm ASPCAP}$, and represent ∼20% of the sample.

Overall, the three methods (G12, N12, RJCE) agree fairly well, within $|\Delta A(K_s)| < 0.2$ mag, while EHK is clearly discrepant. The smallest dispersion relative to this work is seen in comparison to the RJCE method, where even at larger $A(K_s)$ the difference from $A(K_s)_{\rm ASPCAP}$ is smaller than 0.1 mag (compared to a typical $A(K_s)_{\rm ASPCAP}$ uncertainty of ∼0.05 mag). The differences from the G12 maps are centered on zero but have a higher dispersion, with large differences at higher $A(K_s)_{\rm ASPCAP}$ and a set of disparate points with $A(K_s)_{\rm ASPCAP} \lesssim 0.5$. The N12 map predicts similar extinctions as the RJCE values for $A(K_s)_{\rm ASPCAP} < 1$, but the differences become more scattered for larger $A(K_s)$, similar to those found for G12. The EHK method consistently overestimates the extinction, increasing at higher $A(K_s)_{\rm ASPCAP}$.

Figures 5–7 show the extinction offsets as functions of the stellar $T_{\rm eff}$, $\log g$, and [M/H], respectively. While for RJCE only a slight trend with $T_{\rm eff}$ is observed, on the order of the $A(K_s)_{\rm ASPCAP}$ uncertainty for $T_{\rm eff} \lesssim 3800$ K, the EHK method systematically overestimates $A(K_s)$ starting at cooler temperatures ($T_{\rm eff} < 4200$ K). N12 and G12 overestimate $A(K_s)$, compared to ASPCAP, when $T_{\rm eff} > 4500$ K. With respect to surface gravity (Figure 6), EHK systematically overestimates extinction for $\log g < 2$ and G12 and N12 for

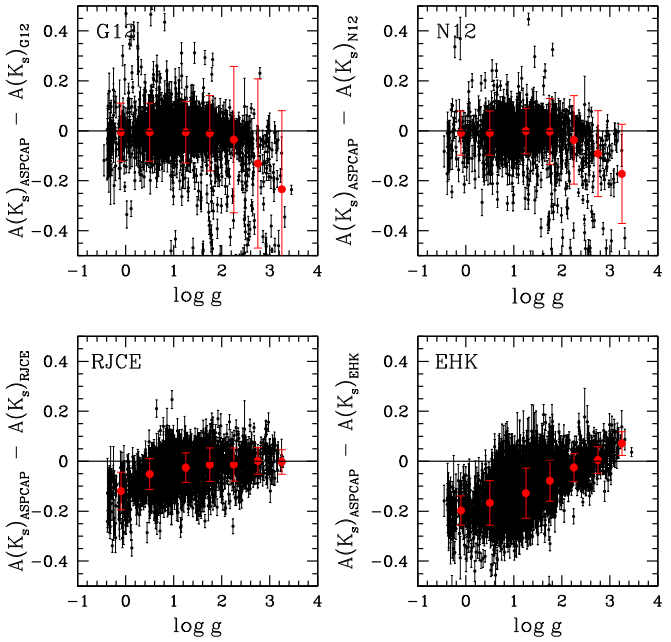

Figure 6. Comparison of our derived extinction, $A(K_s)_{\rm ASPCAP}$, to those of G12 (upper left), N12 (upper right), RJCE (lower left), and EHK (lower right), as a function of $\log g$. The error bars are the results from the isochrone matching (see text). The red points show the median value and dispersion.

(A color version of this figure is available in the online journal.)

$\log g > 2.5$, respectively. RJCE overestimates $A(K_s)$ for the most luminous stars with $\log g < 1$. For [M/H] < -1, the RJCE extinction measurements deviate (Figure 7), indicating that the assumption of a constant $(H-4.5\,\mu{\rm m})_0$ color used in the RJCE estimates is not valid for low metallicities (as also noted in Zasowski et al. 2013), while EHK actually overestimates extinction at higher [M/H]; however, we are limited by the poor statistics for those kind of stars.

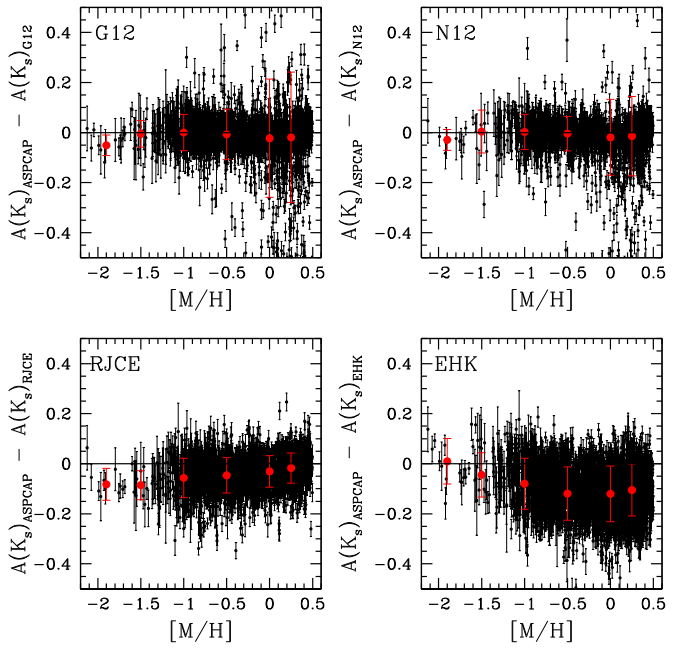

Figure 7. Comparison of our derived extinction, $A(K_s)_{\rm ASPCAP}$, to those of G12 (upper left), N12 (upper right), RJCE (lower left), and EHK (lower right), as a function of [M/H]. The error bars are the results from the isochrone matching (see text). The red points show the median value and dispersion.

(A color version of this figure is available in the online journal.)

In summary, the G12 and N12 maps behave similarly in over-predicting extinction for main-sequence dwarfs and RC or RGB stars with low reddening. Most likely this effect is due to the fact that these maps are heavily weighted by the mean total extinction along the line of sight toward the specific stellar tracers used to make the maps. In both cases, these tracers are stars located in the bulge itself (RC giants for G12 and RGB giants for N12), so any low-reddening foreground sources will be overcorrected by these particular two-dimensional maps (Section 6.1).

Extinctions derived from individual stellar color excesses do not suffer from this problem, since they only measure the impact of dust along the line of sight to each star. In the cases of $A(K_s)_{\rm RJCE}$ and $A(K_s)_{\rm EHK}$, offsets from $A(K_s)_{\rm ASPCAP}$ may be explained by instances where the assumed intrinsic colors are inappropriate for those stellar types. The NIR colors systematically overestimate the extinction, particularly at high extinction, which could indicate that the assumed $(H-K_s)_0$ is offset from the actual mean color of the stars or that the assumed extinction law is incorrect. The dependence of $\Delta A(K_s)$ on the stellar parameters strongly suggests that the offset extinctions are due to the fact that the assumed $(H-K_s)_0$ color is not applicable to all stellar types. As shown by Bessell et al. (1989) and Lançon & Wood (2000), $(H-K_s)_0$ is very sensitive to gravity and metallicity, making the assumption of a single intrinsic color for stars of unknown stellar properties inappropriate. For the stars in our sample, this color appears to be increasingly inapplicable as one moves up the RGB, to lower $\log g$ and $T_{\rm eff}$, with median $A(K_s)$ discrepancies of 0.15 mag for stars with $\log g \lesssim 1.75$ and $T_{\rm eff} \lesssim 4000$ K (corresponding to the common late K giants).

In contrast, the individual RJCE extinction estimates appear to be largely accurate for nearly all stars, with the exception of the coolest RGB stars (M type). The small consistent offset observed ($\lesssim$0.03–0.05 mag) is almost entirely independent of the stellar properties, indicating that a change in the assumed intrinsic color of ∼0.03 mag would remove the discrepancy. We conclude that the RJCE method is the most robust method for tracing interstellar extinction spanning the $T_{\rm eff}$, $\log g$, and [M/H] stellar parameter space studied. However, we do note that if one averages the stellar RJCE extinction values (not just the APOGEE sample, but all bright 2MASS stars) over an area comparable to the N12 and G12 map pixels, the dispersion is comparable to the scatter in Figure 4, strongly suggesting that unresolved differential extinction also has an impact on those map values.

5. COMPARISON TO THREE-DIMENSIONAL MAPS AND MODELS

5.1. Three-dimensional Maps

For comparison to three-dimensional extinction distributions, we use the following data:

1. Marshall et al. (2006) used the stellar population synthesis model of Besançon (Robin et al. 2003), together with the 2MASS data set, to map the three-dimensional extinction for $|l| \leqslant 90°$ and $|b| \leqslant 10°$. Assuming a distance versus color relation (after removing the M dwarf foreground population), they compared the observed stellar colors to the synthetic ones for each line of sight and attributed the resulting reddening to specific distances according to the model. This study is somewhat limited, due to the confusion limit of 2MASS (∼3″ pixels) in the crowded Galactic bulge region and by the sensitivity of 2MASS in highly extinguished regions. The spatial resolution of the map is 15′.
2. Chen et al. (2013) combined the *Spitzer*-IRAC GLIMPSE-II data with the VVV data, along with an improved version of the Besançon model (Robin et al. 2012), to map the inner bulge region ($|l| \leqslant 10°$ and $|b| \geqslant 2°$) in three dimensions. An extension of this map for the entire VVV bulge area ($-10° \leqslant l \leqslant 10°$, $-10° \leqslant b \leqslant 5°$) has been provided by Schultheis et al. (2014). They used an improved color–temperature relation for M giants (using the Padova isochrones; Girardi et al. 2010). In addition, they fit the full color–magnitude diagram including dwarf stars, to the synthetic CMD, to derive the three-dimensional extinction. Their spatial resolution is also 15′.
3. Drimmel et al. (2003) present a Galactic-scale three-dimensional model of Galactic extinction based on the dust distribution model of Drimmel & Spergel (2001), which is fitted to the far- and near-IR data from the *COBE*/DIRBE instrument. The size of the *COBE* pixels are approximately $21' \times 21'$.

Again, if necessary, we rescale all the maps to $A(K_s)$ using the Nishiyama et al. (2009) bulge extinction law.

We queried these three maps for the extinction at the position (l, b) of each of our APOGEE bulge stars, within an FOV of 0.25 deg^2 and in distance bins of 1 kpc. This FOV was chosen to contain a sufficient number of APOGEE stars with accurate stellar parameters at each spatial position. Because the extinction maps have different spatial resolutions, we took the median value around the center position of each 0.25 deg^2 field. Figure 8 shows the comparison of the three-dimensional extinction along different lines of sight, where we compare the literature extinction values (colored lines) with the isochrone-derived $A(K_s)$ values for the APOGEE sources (black points). We indicate also the errors in $A(K_s)$ and distance. Note that, in contrast to Drimmel et al. (2003), the three-dimensional maps

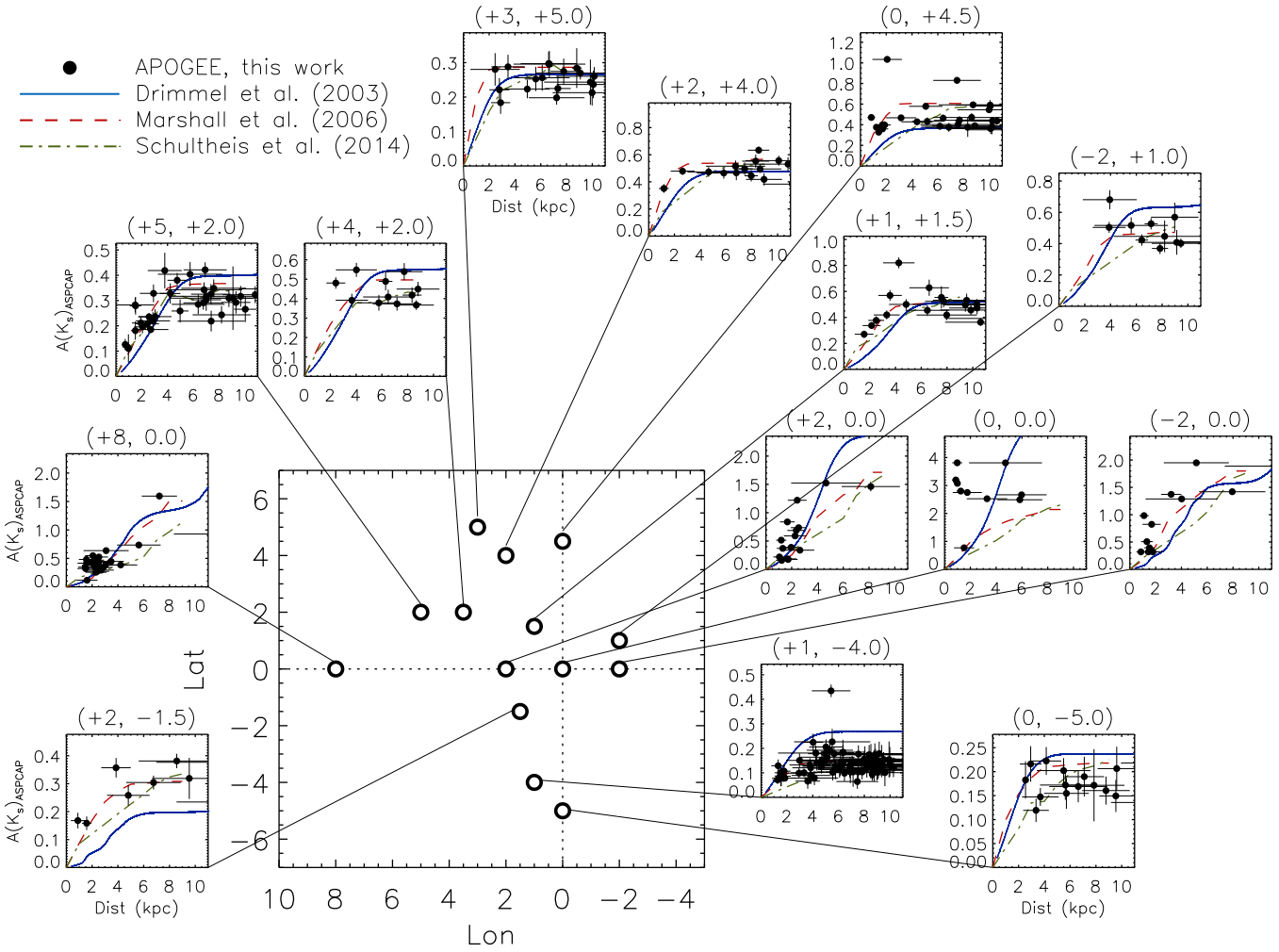

Figure 8. $A(K_s)_{\rm ASPCAP}$, as a function of heliocentric distance (black points), compared to the three-dimensional interstellar extinction maps of Drimmel et al. (2003; solid blue line), Marshall et al. (2006; dashed red line), and Schultheis et al. (2014; dash-dot green line) for multiple lines of sight.

(A color version of this figure is available in the online journal.)

of Marshall et al. (2006) and Schultheis et al. (2014) are limited to a heliocentric distance of <10 kpc.

5.2. Results and Discussion

Figure 8 demonstrates that none of the different three-dimensional models reproduce the global $A(K_s)_{\rm ASPCAP}$ versus distance relations along all available lines of sight. The Drimmel et al. (2003) three-dimensional Galactic dust distribution model has, in general the largest systematic deviation from our observed $A(K_s)$ versus distance relations. Drimmel et al. showed (see their Figure 10) that in the inner disk of the Galaxy, their K_s-band extinction can deviate on the order of 20% compared to extinction derived from 2MASS color–magnitude diagrams.

Along most of the lines of sight, we lack APOGEE stars at distances closer to the Sun than ∼4 kpc. Nevertheless, we note a number of trends.

1. For most of the lines of sight, we confirm the steep rise in $A(K_s)$, with a flattening occurring at ∼4–6 kpc, predicted by all of the three-dimensional distributions. In the highly extinguished regions $(l, b) = (+8°, 0°)$, $(+2°, 0°)$, $(-2°, 0°)$, and $(0°, 0°)$, however, this flattening is not predicted by the models. Unfortunately, we do not currently have a sufficient number of data points to confirm this.
2. The Marshall et al. three-dimensional model appears to best represent the increase of $A(K_s)$ with distance for smaller distances ($d < 4$ kpc), while Schultheis et al. most reliably predicts extinction for larger distances ($d > 4$ kpc). The Marshall et al. map is confusion limited by 2MASS, which produces the sudden decrease in $A(K_s)$ at around 8 kpc.
3. The Drimmel et al. map systematically overestimates extinction in the fields $(l, b) = (+4°, +2°)$, $(-2°, +1°)$, $(+1°, -4°)$, and $(0°, -5°)$, and underestimates for the fields $(l, b) = (+2°, -1.^\circ5)$, $(+1°, +1.^\circ5)$, $(0°, +4.^\circ5)$, and $(l, b) = (+2°, +4°)$.
4. In the innermost bulge region ($|l| \leqslant 2°$, $|b| \leqslant 1°$), despite low number statistics, a steep rise in $A(K_s)$ is detected within 3 kpc of the Sun that is *only* predicted by the Drimmel et al. model.
5. The APOGEE stars in the fields $(l, b) = (0°, -5°)$ and $(+1°, -4.^\circ0)$ span the full range of distance from ⩽2–10 kpc. These low-extinction fields follow the $A(K_s)$ versus distance relation predicted by both Marshall et al. (2006) and Schultheis et al. (2014), while Drimmel et al. (2003) overestimates the extinction, particularly where $d \gtrsim 5$ kpc. Due to the low extinction, however, small spatial variations in $A(K_s)$ cannot be traced with this data set—optical data, with its greater extinction susceptibility, is necessary.

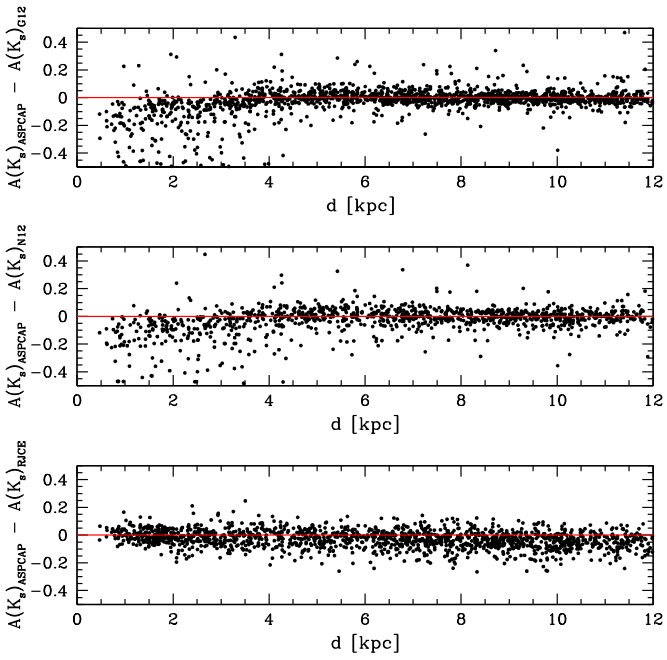

Figure 9. Difference of our derived extinction, $A(K_s)_{\rm ASPCAP}$; to those of G12 (upper panel), N12 (middle), and RJCE (lower) extinction values, as a function of distance.

(A color version of this figure is available in the online journal.)

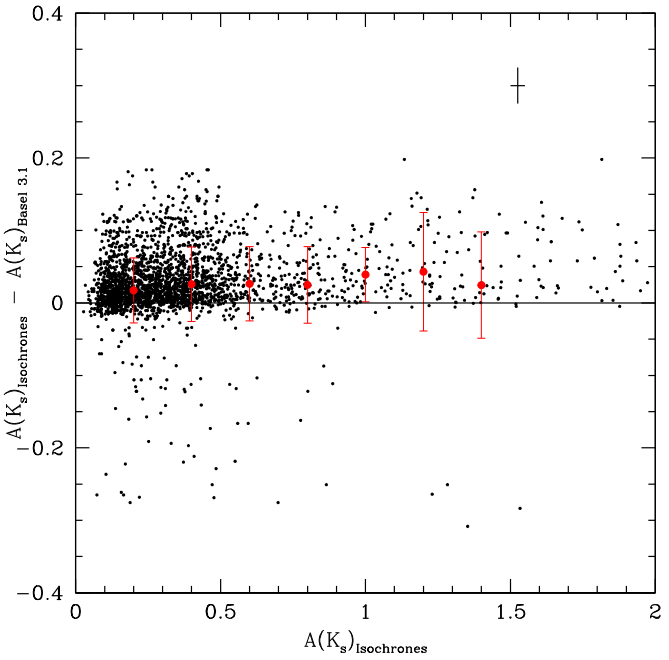

Figure 10. Extinction derived from Padova isochrones compared to those obtained using the Basel3.1 stellar library. The red points indicate the median value of the differences. The typical uncertainty bar is shown in the top right corner.

(A color version of this figure is available in the online journal.)

With additional data from APOGEE and APOGEE-2 in the coming years, we will be able to trace the distance versus $A(K_s)$ behavior toward the full Galactic bulge, making this sample an ideal tool with which to systematically and quantitatively compare spectroscopically derived values with existing three-dimensional interstellar extinction maps, and to better understand the dust structure.

6. ADDITIONAL DISCUSSION

6.1. Two-dimensional versus Three-dimensional Extinction Maps

What are the biases introduced by adopting a two-dimensional extinction map over a more detailed three-dimensional distribution? What are the typical distances probed by two-dimensional bulge extinction maps? In Figure 9, we present the difference in $A(K_s)$ as a function of stellar distance for the two-dimensional maps N12 and G12. Both two-dimensional maps agree remarkably well—with each other and with the ASPCAP extinction—for distances larger than ∼3–4 kpc, while for the shorter distances they systematically overestimate extinction by ∼0.1–0.2 mag (∼0.8–1.6 mag in V-band). This result suggests that for sources known to be in the Galactic bulge, or at least beyond ∼4 kpc from the Sun, these two-dimensional extinction maps can be applied without significant systematic offsets. The RJCE color excess method, which is in theory distance-independent (if not entirely in practice, due to the need for quality stellar photometry), also traces the extinction well for shorter distances, provided the star is not too metal-poor (Section 4.2). Thus, the primary potential bias in the application of two-dimensional maps is for stars along the line of sight toward the bulge, but not established to be in it.

6.2. Dependence on Extinction Law

The derived distances also depend on the extinction law adopted to convert between the reddening measured from the isochrone-matching and the final extinction used in the distance calculation. We assume here the extinction law derived for the Galactic bulge by Nishiyama et al. (2009), with $A(K_s) = 0.526 \times E(J - K_s)$. However, studies have found spatial variations in the extinction-law coefficients even within the bulge (e.g., Udalski 2003, Gosling et al. 2009; Chen et al. 2013; Nataf et al. 2013), which may be due to changes in the dust size distribution (e.g., Draine 2003; Chapman et al. 2009; Zasowski et al. 2009). We tested the impact of adopting a different extinction law and found that, compared to our distance errors from other sources, any shift (even with the standard Cardelli et al. 1989 law) is sufficiently negligible and does not affect our conclusions here. A difference in ∼10% in the extinction law produces a typical difference in the distance estimate of about 5%, which is smaller than our derived errors.

6.3. Differences between Stellar Libraries

The stellar atmosphere models used to produce the isochrones also affect the final extinction values and distances derived for the stars. Here we compare the distances used in this analysis, calculated with the Padova isochrones (Girardi et al. 2010), with those calculated using an identical method but adopting the Basel3.1 model library (Lejeune et al. 1997). We demonstrate the importance of being aware that model libraries do differ, and that the differences can complicate the comparison of results that do not use the same library.

The Basel3.1 library is a semi-empirical, stellar atmospheric library based on the preceding Basel2.2 generation of models (Lejeune et al. 1997) and extended to non-solar metallicities by Westera et al. (2002). The Kurucz theoretical spectra (Kurucz 1979) have been modified to fit broad-band photometry (Buser & Kurucz 1992). As shown by Schultheis et al. (2006), the Basel3.1 library produces reliable color estimates for $T_{\rm eff} >$ 4000 K but shows significant offsets for cooler stars. Therefore,

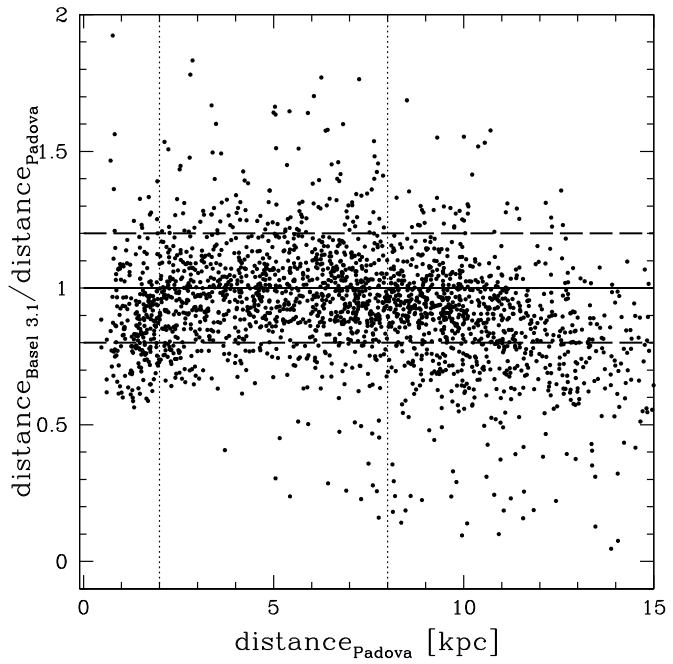

Figure 11. Ratio of distances derived from the Padova isochrones to the Basel3.1 stellar library, as a function of distance. The dashed horizontal lines indicate ±20% error.

we have used complementary NextGen models from PHOENIX stellar atmosphere models (Hauschildt et al. 1997) for stars with $T_{\rm eff} < 4000$ K. As the PHOENIX models use a direct opacity sampling, including over 500 million lines of atomic and molecular species, they yield a more realistic description of the M star population. This composite stellar library is also the one used in the Besançon stellar population synthesis model (Robin et al. 2012).

The effect on the derived $A(K_s)$ of using different stellar libraries is presented in Figure 10. The Basel3.1 $A(K_s)$ values are systematically smaller than the Padova ones, which indicates that the model intrinsic colors are slightly redder than those in the Padova library. However, the effect is typically smaller than 0.05 mag in $A(K_s)$.

Figure 11 shows the comparison in the distances, d, derived using the Padova and the Basel3.1 isochrones. Some systematic difference is apparent, especially for $d \lesssim 2$ kpc and $d \gtrsim 10$ kpc, where the mean Basel3.1 distances are systematically smaller. The typical dispersion is about 20% (indicated by the dashed lines), which is roughly comparable to the intrinsic error of our method (see Figure 3).

Figure 12 traces the distance differences as functions of the spectroscopic stellar parameters. Figure 12(a) reveals a dramatically larger dispersion for stars with $T_{\rm eff} < 3800$ K, which suggests important systematic differences in the stellar atmosphere models between Padova and Basel3.1. (This is close to—but not exactly—where the Kurucz and PHOENIX model atmospheres are merged in the Basel3.1 library.) Similarly, in Figure 12(b), a larger spread in Δd for stars with $\log g < 2$ is found, along with consistently larger distances where $\log g < 0.4$. There are also larger discrepancies when going to lower metallicities ([M/H] $\lesssim +0.25$; Figure 12(c)). Thus, the use of different stellar libraries can produce systematic differences in calculated distances, most significantly for cool, metal-poor M giants. As these stars are often the most distant objects in a magnitude-limited sample of giants, such as APOGEE's, care must be taken in the interpretation of results apparently coming from the distant zones probed by these stars.

7. CONCLUSIONS

Data from the APOGEE survey, which includes stellar parameters ($T_{\rm eff}$, $\log g$, [M/H]) as well as spectra, serve as useful tools to trace interstellar extinction in the most heavily extinguished parts of the Milky Way—the bulge and inner disk. In this paper, we matched the fundamental parameters of 2433 bulge giant stars to model isochrones and derived their extinctions and distances (Sections 2 and 3). We compared these spectroscopically derived extinctions to a variety of theoretical and photometrically derived extinction maps and models (Sections 4 and 5).

Individual stellar extinction estimates derived from long baseline, near- to mid-IR colors (the RJCE method; Majewski et al. 2011) are the most reliable predictors of extinction toward our sample. Extinctions based on near-IR colors only appear accurate for a much narrower range of spectral types, which then requires foreknowledge of (or assumptions about) the stars under consideration before calculating the extinctions. The bulge extinction maps of Nidever et al. (2012) and Gonzalez et al. (2012) perform similarly well in tracing the extinction of stars actually residing in the bulge, but unsurprisingly, overpredict the extinction for foreground sources. For the Nidever et al. (2012) and Gonzalez et al. (2012) maps, "foreground" means stars closer to the Sun than ∼3–4 kpc.

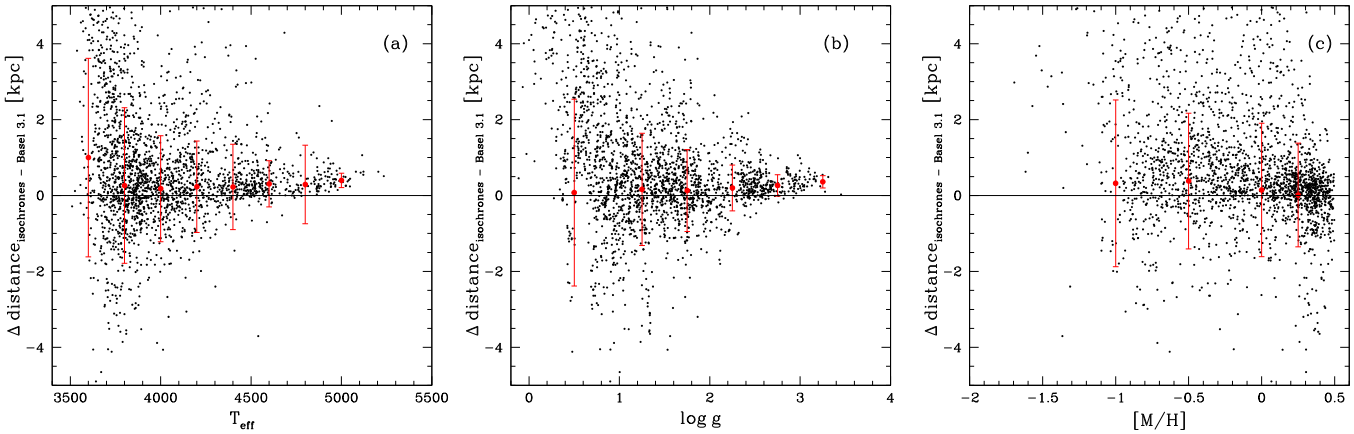

Figure 12. Difference in distances between Padova and Basel3.1, as a function of (a) $T_{\rm eff}$, (b) $\log g$, and (c) [M/H].
(A color version of this figure is available in the online journal.)

We also use our stellar distance estimates to assess three three-dimensional extinction distributions: the model of Drimmel et al. (2003) and the maps of Marshall et al. (2006) and Schultheis et al. (2014). We confirm the steep increase in extinction in the first few kiloparsecs, and the flattening of the extinction at about 4 kpc from the Sun. However, none of the three-dimensional maps agree for all of the APOGEE lines of sight, which demonstrates that there remains significant room for improvement in our knowledge of the three-dimensional bulge extinction distribution.

Finally, we examine additional sources of uncertainty in our comparisons: variations in the adopted extinction law and variations in the isochrones from different stellar atmospheric models (Section 6). Uncertainties due to potential extinction law variations are small compared to uncertainties from the stellar parameters and distance calculations themselves. However, discrepancies in derived extinctions and distances can be substantial if different atmospheric models are adopted, particularly for the coolest (and typically most distant) giants. This caveat should be considered by anyone wishing to compare or combine results that use different atmospheric libraries.

We want to thank the referee for his/her helpful comments. G.Z. has been supported by an NSF Astronomy & Astrophysics Postdoctoral Fellowship under Award No. AST-1203017. T.C.B. acknowledges partial support from support from grant PHY 08-22648: Physics Frontier Center/Joint Institute for Nuclear Astrophysics (JINA), awarded by the U.S. National Science Foundation. MS has been supported by the ANR-12-BS05-0015-01.

Funding for SDSS-III has been provided by the Alfred P. Sloan Foundation, the Participating Institutions, the National Science Foundation, and the U.S. Department of Energy Office of Science. The SDSS-III Web site is http://www.sdss3.org/.

SDSS-III is managed by the Astrophysical Research Consortium for the Participating Institutions of the SDSS-III Collaboration including the University of Arizona, the Brazilian Participation Group, Brookhaven National Laboratory, Carnegie Mellon University, University of Florida, the French Participation Group, the German Participation Group, Harvard University, the Instituto de Astrofisica de Canarias, the Michigan State/Notre Dame/JINA Participation Group, Johns Hopkins University, Lawrence Berkeley National Laboratory, Max Planck Institute for Astrophysics, Max Planck Institute for Extraterrestrial Physics, New Mexico State University, New York University, The Ohio State University, Pennsylvania State University, University of Portsmouth, Princeton University, the Spanish Participation Group, University of Tokyo, University of Utah, Vanderbilt University, University of Virginia, University of Washington, and Yale University.

REFERENCES

Ahn, C. P., Alexandroff, R., Allende Prieto, C., et al. 2014, ApJS, 211, 17
Allende Prieto, C., Beers, T. C., Wilhelm, R., et al. 2006, ApJ, 636, 804
Allende Prieto, C., Majewski, S. R., Schiavon, R., et al. 2008, AN, 329, 1018
Anders, F., Chiappini, C., Santiago, B. X., et al. 2014, A&A, 564, 115
Asplund, M., Grevesse, N., Sauval, A. J., Allende Prieto, C., & Kiselman, D. 2005, A&A, 435, 339
Bessell, M. S., Brett, J. M., Wood, P. R., & Scholz, M. 1989, A&AS, 77, 1
Borucki, W. J., Koch, D., Basri, G., et al. 2010, Sci, 327, 977
Buser, R., & Kurucz, R. L. 1992, A&A, 264, 557
Cardelli, J. A., Clayton, G. C., & Mathis, J. S. 1989, ApJ, 345, 245
Castelli, F., & Kurucz, R. L. 2004, arXiv:astro-ph/0405087
Chapman, N. L., Mundy, L. G., Lai, S.-P., & Evans, N. J., II. 2009, ApJ, 690, 496
Chen, B. Q., Schultheis, M., Jiang, B. W., et al. 2013, A&A, 550, A42
Draine, B. T. 2003, ARA&A, 41, 241
Drimmel, R., Cabrera-Lavers, A., & López-Corredoira, M. 2003, A&A, 409, 205
Drimmel, R., & Spergel, D. N. 2001, ApJ, 556, 181
Dutra, C. M., Santiago, B. X., Bica, E. L. D., & Barbuy, B. 2003, MNRAS, 338, 253
Eisenstein, D. J., Weinberg, D. H., Agol, E., et al. 2011, AJ, 142, 72
Fritz, T. K., Gillessen, S., Dodds-Eden, K., et al. 2011, ApJ, 737, 73
Gao, J., Jiang, B. W., & Li, A. 2009, ApJ, 707, 89
Garcia Perez, A. E., Allende-Prieto, C., Cunha, K. M., et al. 2014, in AAS Meeting Abstracts, Vol. 223, #440.07
Girardi, L., Williams, B. F., Gilbert, K. M., et al. 2010, ApJ, 724, 1030
Gonzalez, O. A., Rejkuba, M., Zoccali, M., et al. 2012, A&A, 543, A13
González Hernández, J. I., & Bonifacio, P. 2009, A&A, 497, 497
Gosling, A. J., Bandyopadhyay, R. M., & Blundell, K. M. 2009, MNRAS, 394, 2247
Gosling, A. J., Blundell, K. M., & Bandyopadhyay, R. 2006, ApJL, 640, L171
Gunn, J. E., Siegmund, W. A., Mannery, E. J., et al. 2006, AJ, 131, 2332
Hauschildt, P. H., Baron, E., & Allard, F. 1997, ApJ, 483, 390
Koesterke, L. 2009, in AIP Conf. Ser. 1171, Quantitative Spectroscopy in 3D, ed. I. Hubeny, J. M. Stone, K. MacGregor, & K. Werner (Melville, NY: AIP), 73
Koesterke, L., Allende Prieto, C., & Lambert, D. L. 2008, ApJ, 680, 764
Kunder, A., Popowski, P., Cook, K. H., & Chaboyer, B. 2008, AJ, 135, 631
Kurucz, R. L. 1979, ApJS, 40, 1
Lada, C. J., Lada, E. A., Clemens, D. P., & Bally, J. 1994, ApJ, 429, 694
Lançon, A., & Wood, P. R. 2000, A&AS, 146, 217
Lejeune, T., Cuisinier, F., & Buser, R. 1997, A&AS, 125, 229
Lombardi, M., & Alves, J. 2001, A&A, 377, 1023
Majewski, S. R., Wilson, J. C., Hearty, F., Schiavon, R. R., & Skrutskie, M. F. 2010, in IAU Symp. 265, The Apache Point Observatory Galactic Evolution Experiment (APOGEE) in Sloan Digital Sky Survey III (SDSS-III), ed. K. Cunha, M. Spite, & B. Barbuy (Cambridge: Cambridge Univ. Press), 480
Majewski, S. R., Zasowski, G., & Nidever, D. L. 2011, ApJ, 739, 25
Marigo, P., Girardi, L., Bressan, A., et al. 2008, A&A, 482, 883
Marshall, D. J., Robin, A. C., Reylé, C., Schultheis, M., & Picaud, S. 2006, A&A, 453, 635
Mészáros, S., Allende Prieto, C., Edvardsson, B., et al. 2012, AJ, 144, 120
Mészáros, S., Holtzman, J., García Pérez, A. E., et al. 2013, AJ, 146, 133
Nataf, D. M., Gould, A., Fouqué, P., et al. 2013, ApJ, 769, 88
Nidever, D. L., Zasowski, G., & Majewski, S. R. 2012, ApJS, 201, 35
Nishiyama, S., Tamura, M., Hatano, H., et al. 2009, ApJ, 696, 1407
Robin, A. C., Marshall, D. J., Schultheis, M., & Reylé, C. 2012, A&A, 538, A106
Robin, A. C., Reylé, C., Derrière, S., & Picaud, S. 2003, A&A, 409, 523
Schultheis, M., Chen, B. Q., Jiang, B. W., et al. 2014, arXiv:1405.0503
Schultheis, M., Ganesh, S., Simon, G., et al. 1999, A&A, 349, L69
Schultheis, M., Robin, A. C., Reylé, C., et al. 2006, A&A, 447, 185
Stanek, K. Z. 1996, ApJL, 460, L37
Sumi, T. 2004, MNRAS, 349, 193
Udalski, A. 2003, ApJ, 590, 284
Westera, P., Lejeune, T., Buser, R., Cuisinier, F., & Bruzual, G. 2002, A&A, 381, 524
Zasowski, G., Johnson, J. A., Frinchaboy, P. M., et al. 2013, AJ, 146, 81
Zasowski, G., Majewski, S. R., Indebetouw, R., et al. 2009, ApJ, 707, 510